Science & Global Security, Volume 9 pp 143-163

0892-9882/01 $12.00 + .00

Monitoring Large Enrichment Plants Using Thermal Imagery from Commercial Satellites: A Case Study

Adam Bernstein[a]

Editor's Note: In issue 8:3, we published an article by Hui Zhang and Frank von Hippel, "Using Commercial Imaging Satellites to detect the Operation of Plutonium-Production Reactors and Gaseous-Diffusion Plants."[1] The study here presents a detailed examination of one of the cases discussed in the earlier article -- that of the U.S. Portsmouth Gaseous Diffusion Plant. As noted by Hui Zhang and von Hippel, subsequent to the completion of their paper, a more detailed analysis of thermal imagery at Portsmouth was carried out by Adam Bernstein. That analysis, a longer version of this paper, is available as a Sandia National Laboratories SAND report.[2]

Thermal imagery from currently operating commercial satellites is an interesting candidate technology for monitoring certain types of fissile material production sites. Potential applications include the Fissile Material Cutoff Treaty (FMCT) or a Fissile Material Production Moratorium. To help determine the capabilities and limitations of such imagery as a monitoring tool, I have examined archived LANDSAT-5 images of the Portsmouth Gaseous Diffusion Plant, a large U.S. uranium-enrichment facility in Ohio. My analysis indicates that large-scale gaseous diffusion plants (GDPs) can very likely be recognized as operational with thermal imagery throughout most of the year in clear weather conditions. It may also be possible to identify certain other large-scale changes in operations, such as the shut-down of a single process building in a plant, by comparing rooftop temperatures of neighboring operational process buildings. However, uncertainties in the current data set prevent a definitive conclusion regarding the latter capability. This study identifies intrinsic weaknesses, including vulnerability to countermeasures, that prevent thermal imagery from satellites (at current resolutions) from being a robust stand-alone verification tool, even for very large plants. Nonetheless, the imagery may be useful to trigger an on-site inspection, to alert and train inspectors prior to an inspection, and to reduce the frequency of on-site inspections

---

The original version of this manuscript was received by *Science & Global Security* on 4 January, 2001.

a Radiation Detection Group, Org. 8418, Sandia National Laboratories, Livermore, CA.

required at a given site. It could have immediate utility for monitoring the two large GDPS in the United States and the French plant at Tricastin, and possibly for determining the operational status of two GDPS in China as well – a total of five plants worldwide. The ease of acquisition and modest cost of thermal commercial imagery further increase its attractiveness as a verification tool.

INTRODUCTION

Reliable monitoring of uranium enrichment facilities, especially those capable of producing high-enriched uranium (HEU), is a key challenge for any regime that would monitor or restrict fissile material production. In this paper I explore the potential of thermal imagery from commercial satellites as a tool for monitoring such facilities. For this purpose, I examined archived LANDSAT-5 images of the Portsmouth enrichment plant in southern Ohio over a ten-year period beginning in 1988.

Existing LANDSAT-5 thermal imagery, as well as imagery from the LANDSAT-7 satellite launched in April 2000, may be helpful in detecting certain large-scale changes in the operational status of GDPs. However, thermal imagery (at virtually any resolution) cannot detect more subtle changes in plant operations – for example, those that might occur if stages within a single process building were reconfigured.

The qualitative change detection capability identified here limits but does not preclude the use of thermal imagery as a monitoring tool. Examples of possible applications include: triggering closer inspections of plant operations; alerting on-site inspectors to possible anomalous activity prior to an inspection; and helping to reduce the frequency of on-site inspections. This last application could be attractive for the United States, since two of the GDPs currently suitable for monitoring with thermal imagery (described below) are located in the United States. Moreover, the modest cost of the commercial images (a few hundred dollars per image in the case of LANDSAT-7) increases the attractiveness of the method, even for these limited applications.

Confounding factors such as wind and other atmospheric conditions can degrade the thermal signature and make interpretation difficult. In addition, the host country might attempt to conceal the heat output of the plant in various ways. Further study is required to determine whether the change detection capability suggested by the current study could be reproduced in an actual monitoring regime.

In the first sections of this paper I identify the available sources of satellite thermal imagery, and the types of enrichment plants most suitable for monitoring with this imagery. Next I review the relevant characteristics of the Portsmouth plant, and describe the factors influencing rooftop temperature

measurement. I then analyze two images of the plant, and conclude with a discussion of the capabilities and limitations of thermal imagery from commercial satellites as an FMCT monitoring tool.

AVAILABLE COMMERCIAL PLATFORMS

The only commercial sources of thermal imagery currently available are the LANDSAT satellites, LANDSAT-5 and LANDSAT-7. This study relies only on LANDSAT-5 data, which has a 120x120 m pixel size. Thus, a typically sized GDP building of a dozen hectares or so is covered by only 10 to 15 pixels. LANDSAT-7 was launched in April of 1999, and has 60 m spatial resolution in the thermal band,[3] increasing the number of pixels by a factor of 4. The nominal thermal resolution for both LANDSAT-5 and LANDSAT-7 is around 0.5-1 °C, once atmospheric and other effects are accounted for.[4] Overall temperature *shifts* of several Celsius degrees are possible if the systematic temperature effects are not corrected, but will not affect the relative measurements to be used in this study. For this LANDSAT-5 data set, a resampling procedure implemented by the image supplier may have degraded the resolution, even for relative measurements, to as much as a few degrees Celsius. This effect, discussed in detail in reference 2, is an artifact of the current data set and can be avoided in other data sets and platforms.

Although not a directly commercial platform, another potential source of imagery is the ASTER imaging system,[5] scheduled for a November 1999 launch with the NASA EOS AM-1 satellite. ASTER has a spatial resolution in each of its five thermal bands of about 90 m. ASTER data will be made publicly available (though with some restrictions) through NASA's EOSDIS program.[6]

ENRICHMENT PLANTS SUITABLE FOR MONITORING WITH THERMAL IMAGERY

Global uranium enrichment capacity is dominated by gaseous diffusion and gas centrifuge technology. With a specific power consumption of about 2400 kWh/SWU,[7] gaseous diffusion is the most energy intensive enrichment method, and GDPs are among the largest roofed buildings in the world. This combination of properties makes them good candidates for monitoring with thermal imagery. In contrast, the energy consumption of a gas centrifuge plant is about 10 times lower than that of a gaseous diffusion plant of equal

enrichment capacity. The roof area of a gas centrifuge plant is also about 10 times smaller than that of a diffusion plant of equal capacity. This area corresponds to no more than one unresampled spatial pixel in the LANDSAT-5 thermal band,[8] or about 4 pixels in the LANDSAT-7 thermal band.

There are two large operational GDPs in the United States, the Paducah and Portsmouth plants. France has one operational plant at Tricastin. One or possibly two GDPs operate or have operated in China, at Lanzhou and at Heiping.[9]

Given the comparatively small area and low heat output of other types of enrichment plants, monitoring of enrichment plants with the thermal imagery currently available from commercial sources is essentially restricted to GDPs. The smallest GDP, the Chinese plant at Lanzhou, (approximately 700 m by 100 m in size, or six pixels) is barely visible using LANDSAT-5, but would span about 24 pixels in a LANDSAT-7 image. Using 10 pixels as a rough figure of merit for detection of an operating plant, relaxing the restriction to GDPs would require further improvements in the spatial resolution of commercial satellite imagery, by a factor of about two beyond LANDSAT-7's 60 m resolution.

DESCRIPTION OF THE PORTSMOUTH GASEOUS DIFFUSION PLANT

The Portsmouth GDP was a dedicated government HEU production facility until 1992, when it was adapted to the purpose of civil production of low enriched uranium (LEU). The plant produced ~90% enriched HEU through November 20, 1992, after which it began producing LEU enriched to the 4-5% level. For convenience, I refer to the earlier operational state as the "HEU mode" and the later state as the "LEU mode."

The plant, shown in Figure 1, has three separate process buildings, numbered 326, 330, and 333. Each building has two floors, with the second floor housing the process equipment. Buildings 330 and 333 have an area of about 9 pixels (13 hectares) while building 326 has a roof area of about 8 pixels (11.4 hectares). The cascade begins in building 333, which contains 640 stages. The amount of process material is largest in the earlier stages, and the stages in this building are therefore the largest and most energy intensive. Building 330, containing 1100 stages, is the next step in the cascade, enriching the uranium to around the 4-5% level. In the HEU mode, the final enrichment to more than 90% was accomplished in building 326, which housed about 2280 stages. According to plant records, about 85-90 percent of the stages in this building were shut down in 1994, relative to the number operational in 1991.

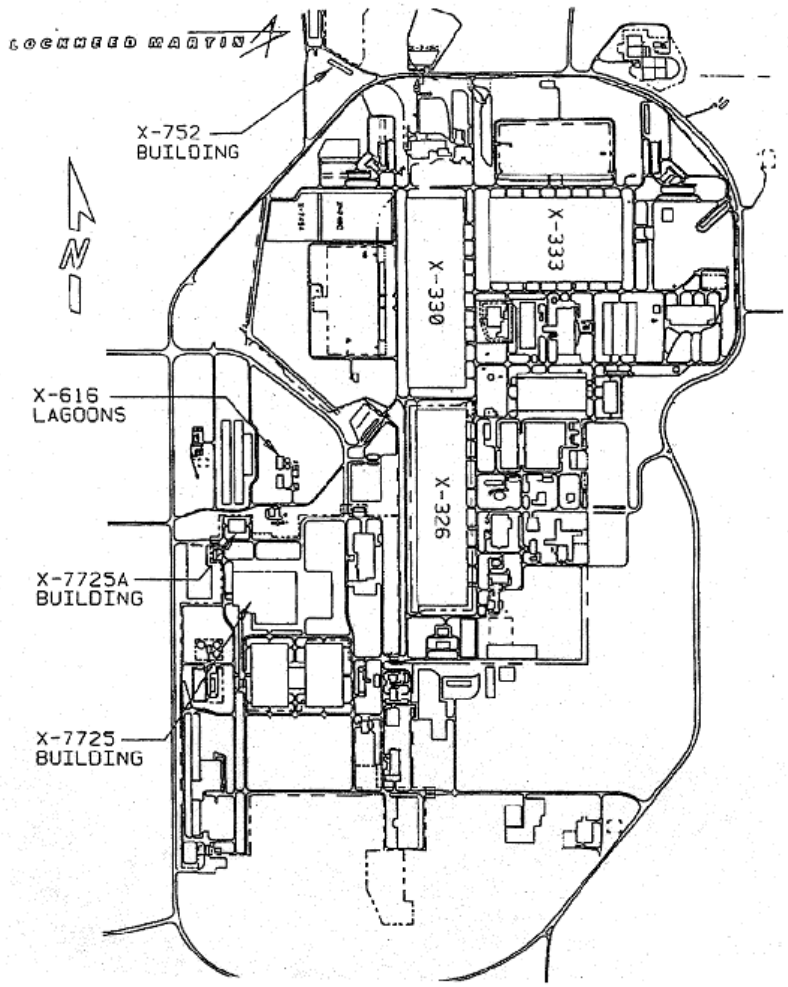

Figure 1: The Portsmouth gaseous diffusion plant.

For this study, the physical parameter of interest is the emitted radiant energy. The sources of this energy are the stages themselves, heaters (used to maintain the gas temperature in process piping), power supplies, and other building utilities. The roof temperature is also strongly affected by solar heating and by the wind, as discussed below.

Each building has its own recirculating cooling water system connected to an evaporative steam cooling tower. One tower is located near the northwest corner of building 330 and the other two are near the northeast corner of building 333. Building ventilation is achieved with cooling air pulled in

through filters on the ground floor and pushed to the second floor through floor vents and openings in the cell motor bases. Hot air from the second floor is vented through numerous controlled roof vents, lowering the interior ceiling temperature and the rooftop temperature. The process building roofs are several inch thick multi-layers consisting of tar, paper, insulation, and gravel on top of their steel roof decking.[10] The actual value of the roof emissivity was not measured for this study. I used a nominal value for the roof's thermal emissivity of 0.9, basing this estimate on the range of values for concrete, rock, and brick.[11]

It is important to compare the size of the temperature increase expected from internal activities with the approximate few Celsius degrees resolution (for relative measurements) of the satellite imaging system. From discussions with Portsmouth officials,[12] and from other sources,[13] I adopt a value of 60 °C for the internal ceiling temperature. As shown in detail in reference 2, Appendix I, this internal temperature would produce characteristic rooftop temperatures of about 18 °C for an outside air temperature of 4 °C, and 41°C for an ambient temperature of 35 °C. (absent solar heating). The temperature difference relative to ambient arising from internal activity is therefore never less than 5-6 °C in the worst case (the summer), and is typically 10-15 °C or greater. Changes of this magnitude will be easily detectable with any of the platforms described above, including LANDSAT-5.

As discussed below and in reference 2, Appendix I, wind and solar heating significantly alter the apparent temperature of the rooftops. These effects, though significant in an absolute sense (even at 9:45 AM when the images are acquired), will not obscure the large temperature rise relative to ambient caused by internal activity.

IMAGE ACQUISITION AND ANALYSIS

Data Search

I searched an online archive of LANDSAT images of the Portsmouth plant.[14] From 1988 to 1998, I found about 200 images. After rejecting those with more than 20% cloud cover, for which online previews were unavailable, or which had corrupted data, 50 images remained. From these I chose two: one from February 16 1991, when the plant was operating in HEU mode, and one from

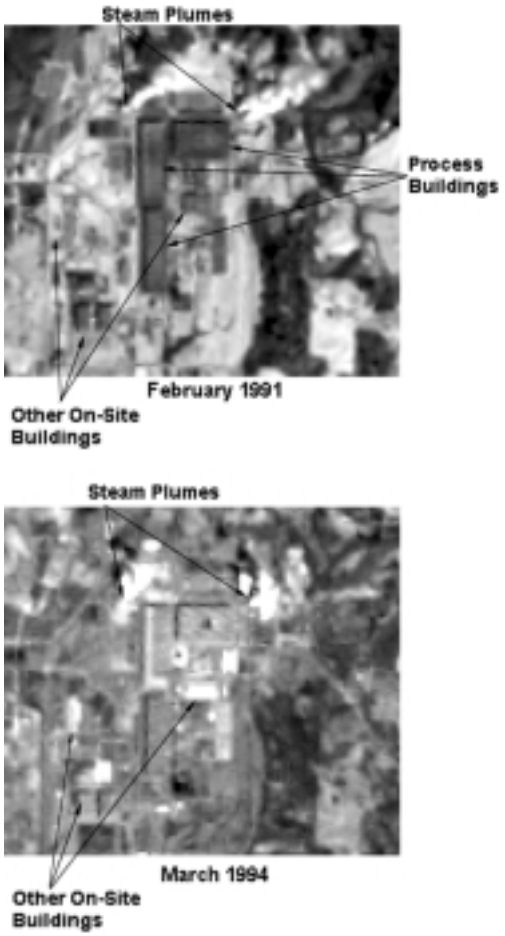

Figure 3: February 16, 1991, and March 12, 1994 visible LANDSAT images of the Portsmouth enrichment plant. Steam plumes from cooling towers can be seen in both images, revealing differing wind patterns. Also shown are relatively large non-process related buildings.

March 12 1994, when the plant was operating in LEU mode.

Information from the Visible LANDSAT Bands

Figure 3 shows images of the plant derived from the LANDSAT visible bands. The process buildings can be seen in both the 1991 and 1994 images, and in all spectral bands including the thermal. Steam plumes from the cooling towers can also be seen in both images, revealing a clear difference in wind conditions. The 1991 image shows a breeze blowing in a northeasterly direction,

while the 1994 image shows relatively little wind. Table 1 summarizes the weather conditions on each day, as recorded in Waverly (a town about 12 km north of the site). The change in external conditions has an important impact on the thermal signature.

Table 1: Ambient conditions at the Portsmouth plant on the days the images were acquired.

Date/Time	Mode	Low temperature (°C)	High temperature (°C)	Wind
February 16, 1991	HEU	- 15	- 7	Breeze to NE
March 12, 1994	LEU	1	10	calm

Factors Affecting the Temperature Measurement

Radiance is the quantity actually measured by thermal sensors on the satellite. The radiance R is defined as the density of the emitted radiant energy in a given spectral range measured at the satellite in watts per square meter. R can be related to the roof surface temperature using a standard algorithm.[15] The goal is to infer activity within the building from the derived roof temperature. However, the temperature can be affected by several factors that do not depend on internal activity. These are discussed briefly here and in more detail in reference 2.

1. **Emissivity.** Emissivity must remain constant to within a few percent between image acquisitions (or be re-measured for each observation). In practice, a monitoring regime would have to include an initial characterization of the emissivity of each process building roof, as well as periodic verification that the value had not changed by more than a few percent.[16] This could be done during on-site inspections. Evidence of emissivity changes taken from the visible/near-infrared bands might be also used to trigger inspections.

2. **Atmospheric interference**. Variations in the transmittance of the atmosphere (due to humidity, cloud cover, and temperature changes) and variation in the background radiance from the atmosphere all affect the apparent temperature of surface objects. As long as atmospheric effects are uniform across the buildings and their surroundings, these shifts will vanish in the relative temperature measurements used in this study. However, care must be taken to select low humidity, cloud and haze-free measurements. In an actual

regime, local weather data could be used to help select suitable images.

3. **Finite pixel size and resampling.** Because the measured radiance within each 120 m pixel is an average over its area, the radiance values of the cooler areas surrounding the buildings will tend to decrease the apparent radiance of the building. In addition, the images used here were resampled by the vendor, or smoothed, with a cubic convolution algorithm as described in Appendix III, reference 2. Resampling can also change the apparent value of the radiance of pixels within the building perimeter. For the current images I estimate that these effects in tandem produce an overall systematic ~2 °C downward shift in building rooftop temperatures. The averaging and resampling problems found in LANDSAT-5 data will be largely eliminated in LANDSAT-7 imagery, since the latter's pixel is 4 times smaller, and since LANDSAT-7 data can be delivered unresampled.

4. **Convection.** Wind and the process building venting system can conspire to reduce the building rooftop temperatures. A crude treatment of convection effects on heat transfer (found in reference 2) shows that a steady uniform 6.7 m/sec (15 mph) wind could reduce all reconstructed rooftop temperatures by about 15 °C. As will be shown, the buildings can still be seen above background even under such conditions. However, unlike previous effects, it is unreasonable to expect the effect of wind to be uniform across all buildings. In practice, images with too much wind would have to be discarded as unreliable. If necessary, the steam emerging from the cooling towers, or local ground truth measurements could be used to select images with little wind.

5. **Solar heating**. An hour or so after sunrise, solar heating begins to contribute significantly to the total heat load in the process building roofs. As discussed earlier, with reasonable assumptions about internal temperatures and heat transmission properties of the roof, internal activity causes a temperature rise above ambient of at least 5 °C, and typically 10-15 °C or more throughout most of the year. Solar heating can contribute another 10-15 °C to the temperature difference from background, but will never completely obscure the effect on the rooftop temperature from internal activity. Nighttime or early-morning images can be acquired if necessary, to reduce or eliminate solar heating effects. Differences between building temperatures could be brought about by selective shading of the rooftops from clouds, haze or other effects, or by non-uniform solar absorptivities. However, such changes would not affect the basic capability of determining the overall operational status of the plant.

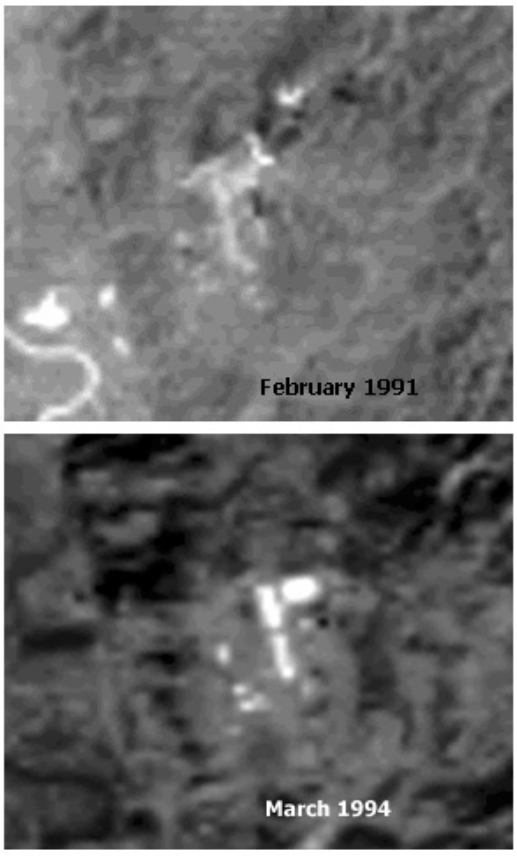

Figure 5: A subset of the 1991 and 1994 thermal band showing the Portsmouth plant signature. In the lower left corner, the markedly different relative values of the radiance of the nearby Scioto River can be seen.

Metrics for Detecting Internal Activity

I employed two metrics to identify internal activity:

1. $T_i - T_0$, with T_i the average reconstructed surface temperature of the ith process building and T_0 the scene average or nearby ground temperature; and,
2. $T_i - T_j$, with T_i and T_j are the average reconstructed surface temperatures of the ith and jth process buildings.

The use of temperature differences removes overall shifts in the measure-

ment. However, non-uniform changes in the emissivity and atmospheric properties are possible, and could result in misinterpretation. Moreover, without ground truth measurements, a nominal value for the emissivity must be assumed in order to reconstruct building temperatures.

Analysis of the Thermal Bands

Figure 5 shows the LANDSAT-5 thermal images of the plant and the surrounding area for both 1991 and 1994. The three process buildings 326, 330 and 333 can be clearly seen in the center of each image above the surroundings. This qualitative identification is based only on the different radiance values of the buildings and the background, and does not depend on any assumptions about the emissivity or the temperature calibration. Overall, the rooftop radiance in the "HEU-mode" 1991 image is lower than in the "LEU-mode" 1994 image. This is due to the significantly lower ambient temperature and heavier wind conditions in the earlier image.

The 1991 image provides useful evidence of the adverse effects of wind on the thermal signature. In that image, the wind blurs and degrades the thermal signatures of the process buildings. Steam emerging from the cooling towers northeast and northwest of the process buildings is spread by the northeasterly wind. This effect could obscure temperature differences if the wind were to blow steam directly across the process building roofs. In the 1994 thermal image the effects of the wind are smaller and the building edges appear sharper, a difference consistent with the different wind patterns evident in the visible bands.

Figure 7 shows a perspective relief map made from the thermal band. The height of each feature is proportional to the raw pixel value in the thermal band, with a scaling factor of 20 applied to enhance the contrast. The dark areas in the image, located near building boundaries indicate sharp changes in the radiance. There is a qualitative appearance of variation in radiance between process buildings in the 1994 image, while in the 1991 image all buildings appear to be at roughly the same radiance values. In the 1994 image, the average radiance of building 326, in which a significant reduction in activity is known to have occurred, has dropped relative to the other two buildings. Building 333, in which little change in activity has occurred, has higher radiance values than its neighbors. To refine the analysis, I reconstruct the temperatures of the process building rooftops, and use the relative metrics defined above.

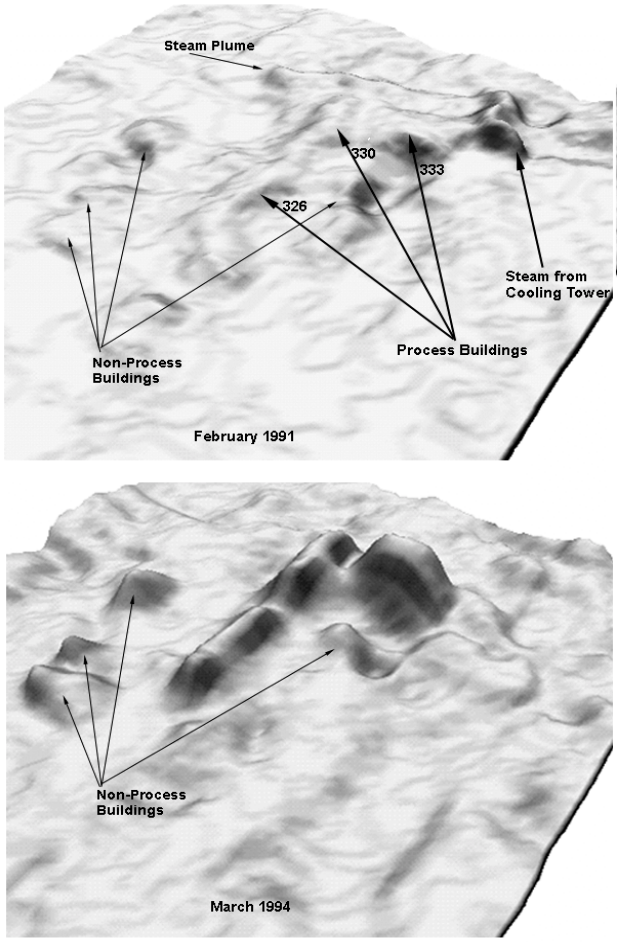

Figure 7: Relief images of the thermal output of process buildings derived from the LANDSAT thermal band. A scale factor of 20 has been applied to all pixels in both images to enhance visibility.

Reconstructed Temperatures of the Process Buildings Relative to Surroundings

An identical temperature reconstruction procedure was followed for both images. The building perimeters were first defined using the visible and near infrared bands. A uniform central interior area was defined for each building, consisting of 30 resampled 28.5 x 28.5 m pixels. A standard algorithm[17] was used to convert the radiance values of each pixel within this area to temperature values. The procedure was performed on data without geocorrection, so

that the only data-related effects are the mixed pixel and resampling effects previously discussed. The temperature is not corrected for any uniform shifts discussed earlier, and assumes a nominal emissivity value for gravel of 0.9.

Table 3 shows the average rooftop temperature and the rooftop temperature relative to background for each building and for both images. A significant potential nonuniform systematic shift is from resampling and pixel averaging, which could induce as much as a ~2 °C downward shift in the reconstructed temperature. This effect, considered in detail in reference 2 is likely to be largest in building 326. In addition, a non-uniform change in emissivity of 5 percent for any building could result in a 2-3 °C shift in its temperature, opposite in sign to the emissivity shift. The last column of the table shows, T_i-T_0, where T_0 is the scene average temperature and T_i the average surface temperature of the ith building. The last row of the table shows the entire scene average temperatures for both images. The scene average temperatures are within their respective ambient temperature ranges as recorded at the weather station (Table 1), providing a rough check on the temperature calibration.

Table 2: Mean values of the recorded surface temperature of each process building roof, using a constant interior area of 30 pixels = 24367.5 m^2. The emissivity is assumed to be 0.9 throughout. A nonuniform systematic shift of as much as 2 °C can occur from the combination of resampling and mixed pixel effects. In addition, nonuniform changes in the emissivity at the 5 percent level could cause shifts of 2 °C (See text above).

Building number	pixels used in mean (28.5 x 28.5m)	Building roof mean temperature and difference from background (T_i-T_0) (ε = 0.9)			
		1991 image		1994 image	
		T_i (°C) error (stat. only)	$T_i - T_o$	T_i (°C) error (stat. only)	$T_i - T_o$
333	(3x10 pixels)	4.1 ± 0.3	+11.8	26.1 ± 0.7	+21.7
330	(2x15 pixels)	3.9 ± 0.4	+11.6	24.1 ± 0.5	+19.7
326	(2x15 pixels)	3.4 ± 0.2	+11.1	22.1 ± 0.6	+17.7
Scene average	(ε = 1)	-7.7°C		4.4°C	

Estimated Contributions from Internal Activity, Solar Heating and Wind

For monitoring with thermal imagery to be effective, it is important to establish that the temperature measurements in Table 3 are produced in significant part by internal activity. Using basic heat transfer equations along with standard values for solar heating and the effects of wind, I have calculated the expected contributions from each source as follows.

Equating the heat flow through the roof, Q_{roof}, to the heat flow by convection and radiation into the ambient air, Q_{air} gives:

$$Q_{roof} = K \times \left(\frac{T_{int} - T_{roof}}{\Delta x} \right) = Q_{air} = C \times (T_{roof} - T_{air}) + \varepsilon\sigma({T_{roof}}^4 - {T_{air}}^4)$$

with

$\varepsilon = 0.9$	→	the roof thermal emissivity;
$\sigma = 5.667 \times 10^{-8} W/(m^2 \circ K^4)$	→	the Stefan-Boltzmann constant;
$\Delta x = 0.1 m$	→	the roof thickness[18];
$K = 0.5 W/(m\ ^\circ C)$	→	the roof heat conductivity;
$C = 10 W/(m^2\ ^\circ C)$	→	the heat transfer coefficient for still air.

This equation assumes no solar heating and that the air above the roof is still. The value of K is chosen as that of a fairly good insulator, while the heat transfer coefficient is a representative value for free convection in air.[19]

T_{int} and T_{air} are respectively the assumed interior temperature of the building at the ceiling, and the assumed ambient temperature above the building. As discussed previously, I adopt a 60-80°C range for the interior temperature T_{int}, based on references 11 and 12. Substituting a range of reasonable values for T_{air} and solving for the roof temperature gives the values for T_{roof} shown in Table 3.

Table 3: The rooftop temperatures T_{roof} of process buildings and their difference from ambient temperature (T_{roof}-T_{air}), for different values of the internal and ambient process building temperatures T_{int} and T_{air}.

T_{int} (°C)	T_{air} (°C)	T_{roof} (°C)	(T_{roof} - T_{air}) (°C)
60	4	18	14
60	15	26	11
60	35	41	6
80	0	20	20

This equation does not account for solar heating, or for the forced venting of heat through holes in the roof surface. The true thermal conductivity of the composite roof is also uncertain, as is the true internal temperature of the building. Nonetheless, the table gives a rough idea of the temperature changes induced by internal activity. As seen in the table, even in very hot summer conditions (T_{air} = 35 °C) the rooftop temperature is still 6 °C above ambient assuming a 60 °C interior ceiling temperature. Since the thermal imagery is sensitive to temperature differences of a few Celsius degrees, this worst case gives confidence that the heating effects due to internal activity can be seen throughout the year.

A full treatment is found in reference 2, Appendix I, including corrections for the effects of solar heating and wind cooling. Assuming a 60 °C internal temperature, and a scene average temperature of 4.4 °C, the predicted rooftop temperature due to internal activity alone is 18 °C for the 1994 data. If in addition to these conditions, the roof has a solar absorptivity value of 0.25, and solar exposure or insolation of 330 W/m^2 [20] the rooftop temperature rises to 23 °C, close to the temperatures actually measured in 1994.[21] Finally, considering the 1991 data in which the effects of wind are apparent, I assume a 6.7 km/sec (15 mph) wind, which causes a 14 °C downward shift in the temperature, for a net temperature of about 10 °C. Again the rough agreement with the 1991 data is fortuitous, enforced by the choice an appropriate wind speed, but the result nonetheless indicates the size of the effect. The important conclusion is that internal activity accounts for a significant portion of the observed temperature rise above background. Despite the potentially large effects from wind and sun, the difference from background caused by internal activity is still far greater than the few Celsius degree resolution of the LANDSAT platforms. Moreover, the effect of wind can be mitigated by a suitable choice of images.

Reconstructed Temperature Differences Between Buildings

Table 4 shows the difference in temperature between buildings, with statistical error added in quadrature, for both images. If the systematic shifts are in fact constant across buildings and images, then the 1994 image reveals a ~4 °C, 4 standard deviation shift in the temperature of building 326 relative to 333, when compared to the 1991 temperature difference between the same pair of buildings. The differences between the other two pairs of buildings are smaller, about 2 °C. The apparent relative drop in temperature in building 326 is qualitatively consistent with ground truth, since about 90 percent of the stages in building 326 are known to be non-operational.

Table 4: T_i-T_j, the difference in reconstructed average building roof temperatures in both images. The systematic effect due to resampling may not be uniform, and could reduce the temperature differences with building 326 by around 2 °C. This could eliminate the apparent difference in the building temperatures.

Building numbers i,j	Difference in building roof mean temperatures (T_i-T_j) (ε = 0.9)	
	1991 image	1994 image
	°C ± (stat error) - est. resampling shift[a]	°C ± (stat error) - est. resampling shift[a]
333,330	0.2 ± 0.5 – 1	2.0 ± 0.9 – 1.0
330,326	0.4 ± 0.5 – 1	2.0 ± 0.8 – 1.0
333,326	0.6 ± 0.4 – 2	4.0 ± 1.0 – 2.0

Because of the apparent consistency between the image analysis and ground truth, one possible conclusion is that the relative temperature change in building 326 from 1991 to 1994 is in fact the effect of the large-scale change in operations. A significant change in the relative mean temperatures of the buildings (i.e., a change correlated to the changes in building activity known from ground truth) can be inferred from the images only if the effects of resampling, pixel mixing, wind and atmospheric interference were uniform across buildings in each image, and only if emissivity changes were constant across both buildings and images. This prevents conclusive use of the relative temperatures of the buildings (T-i-Tj) in the current case. It does not affect the capability of recognizing any particular building as operational in comparison with background using the metric (T_i-T_0).

DISCUSSION

Given that the process buildings are clearly visible in the thermal bands of both images, the above analysis shows that thermal imagery from commercial satellites can reveal that a GDP appears "hot" relative to surroundings, and by implication that the shut-down status of a plant could be identified. In both 1991 and 1994, the thermal images reveal that the buildings are significantly hotter than background – well above the few Celsius degree limits imposed by resolution, and even when the effects of wind and solar heating are accounted for. However, the current image set does not directly show how any of the buildings would appear in the absence of internal activity.

Because a significant proportion of the rooftop heat load is from the sun, even a completely shutdown building would have a temperature well above the surrounding background. This is simply due to the fact that the hollow buildings do not absorb and dissipate heat as efficiently as the surrounding earth, which is an effective heat sink. Nighttime or early morning thermal imagery, might be used to minimize the effects of solar heating and confirm the source of the effect. But even without such imagery, the ~5 – 20 °C increases in roof temperatures induced by internal activity alone (see reference 2, Appendix I) can be clearly seen with existing and future satellite thermal images.

The analysis also suggests, but does not prove, that thermal imagery may be able to reveal that a process building a few hectares in size has been shut down, or nearly so, by examining its temperature relative to other process buildings and to surroundings before and after the shut-down. However, because of the unfavorable wind conditions in the earlier image, and because of the possibility of non-uniform changes across buildings from the principle sources of error, I cannot definitively conclude from the current set of images that this is possible.

In a future study (or an actual regime) three important conditions, all achievable, would have to be met to allow definitive conclusions concerning changes in rooftop temperatures. First, occasional measurements of the emissive properties of the roofs would be required, to ensure that the observed effects were not due to non-uniform emissivity changes. Second, only images in which clear, calm, low haze and humidity conditions prevail could be accepted for analysis. Third, the effects of pixel averaging and resampling would have to be minimized by using higher resolution data and a different (or no) resampling method. The fourfold decrease in pixel area and nearest-neighbor resampling option available for LANDSAT-7 images will largely eliminate the latter effects. Taken together, these refinements would probably allow

detection of a several degree shift in relative temperature between process buildings. In addition, acquisition of nighttime thermal imagery would be useful for removing or minimizing the significant effects of solar heating on the rooftops. Nighttime images of a given region are in principle available at a rate equal to daytime images for the LANDSAT satellites. Change detection with nighttime images is complicated by the fact that it is difficult or impossible to determine building outlines from the visible LANDSAT bands. Still, if used in conjunction with temporally close daytime images, the enhanced contrast in the thermal bands might provide further useful information on the operational status of enrichment plants. Study of such imagery would be a useful follow-on to the current analysis.

Image Availability

This study found a total of about five candidate images per year at this site, after rejection of cloudy and otherwise unsuitable images. This figure may be an underestimation, since not all of the archived images were available for previewing in the online search engine used for this study. The maximum possible rate of daytime image acquisition for LANDSAT-7 is about 22 per year, with this number doubling if nighttime imagery proved useful. Given that major changes in operations at a GDP, such as the restart of a process area, will in practice take at least several months, a repeat rate of five to ten clear images per year appears frequent enough to ensure that such changes do not go undetected.

Countermeasures

There are a variety of ways to deliberately alter roof temperatures so as to hide the effects of a change in plant operations. Some examples include:

- Returning enriched product from the end of an LEU cascade to its initial stages. This process is known as batch recycle.[22]
- the presence of unrelated heat sources in or near the process building;
- strategic placement of process cooling towers;
- changes in the emissivity of the process building roofs;
- changes in building cooling or insulation, and;
- removal of heat to other areas of a multipurpose plant to disguise increased activities in process buildings.

CONCLUSIONS

The current analysis indicates that thermal satellite imagery has utility, albeit limited, as a companion monitoring technology for fissile material production monitoring regimes. There are five GDPs worldwide for which the method might have some immediate use. While LANDSAT-7 will improve the monitoring capability for these plants, it will not allow the expansion of the method to gas-centrifuge plants. As discussed earlier, this would require a factor of 2 or so improvement in spatial resolution beyond LANDSAT-7 (assuming a minimum detectability requirement of ten pixels). Moreover, some ground truth data, most notably periodic measurements of the emissivity of the building roofs, would be required to validate any observed changes.

With those reservations, thermal imagery can still potentially fulfill three useful monitoring functions for any of the GDPs mentioned. It could help reduce the frequency of on-site inspections, prepare inspectors for an imminent site visit, and possibly serve as a trigger for an on-site inspection or an investigation by some other means. In addition, the utility of the method is enhanced by the low cost of the data, a few hundred dollars per image in the case of LANDSAT-7. However, it is clear from the current study that existing thermal imagery cannot be expected to be a robust stand-alone monitoring tool, but should instead be seen as one element in a comprehensive verification regime.

ACKNOWLEDGMENTS

This research was supported by the Cooperative Monitoring Center at Sandia National Laboratories. Sandia is a multiprogram laboratory operated by Sandia Corporation, a Lockheed Martin Company, for the United States Department of Energy under Contract DE-AC04-94AL85000.

The author would like to thank Lynn Calvert, John Shoemaker and Sandy Childers at the Porstmouth plant for providing important information about plant operations. I also benefited greatly from discussions and editorial review by Tom Budge, George Baldwin, Frank Von Hippel and Marty Abrams. Finally, thanks are due to Bill Ballard, Doug Henson and Larry Brandt for facilitating the release of this report. The opinions expressed herein are those of the author alone.

NOTES AND REFERENCES

1. Hui Zhang and Frank N. von Hippel, "Using Commercial Imaging Satellites to Detect the Operation of Plutonium-Production Reactors and Gaseous-Diffusion Plants," *Science & Global Security*, (November 2000): 8:3, 261-313.

2. Adam Bernstein, "Monitoring Large Enrichment Plants Using thermal Imagery from Commercial Satellites: A Case Study," Sandia Report SAND2000-8671, Sandia National Laboratories/CA: May, 2000.

3. http://geo.arc.nasa.gov/sge/landsat/landsat.html.

4. LANDSAT satellite images have seven distinct spectral bands. Three of these are in the visible spectrum, two in the mid-infrared, and one each in the thermal infrared (10-12 µm) and near infrared. The entire image covers a 170¥185 km area on the ground. ~0.5°C resolution has been achieved in practice when atmospheric and emissivity effects are correctly accounted for. See for example, Wukelic et. al., "Radiometric Calibration of LANDSAT Thematic Mapper Thermal Band," *Remote Sensing of the Environment*, (1989): 28, 339-347, in which LANDSAT thermal resolutions of less than 0.5 °C are presented.

5. http://asterweb.jpl.nasa.gov/asterhome.

6. http://asterweb.jpl.nasa.gov/asterdata/authorization/default.htm.

7. SWU stands for a Separative Work Unit, a measurement of the enrichment capacity of the plant.

8. A technology now under development, atomic vapor laser isotope separation (AVLIS), has a specific energy consumption approximately 100 times lower than that of gaseous diffusion. Although no plants of this type have yet been built, they would be all but impossible to identify with low-resolution satellite imagery.

9. Defense Intelligence Agency, *People's Republic of China Nuclear Weapons Employment Policy and Strategy*, 1972. http://www.fas.org/irp/dia/product/prc_72/app_e.htm.

10. Personal Communication, Lynn Calvert, Lockheed Martin Utility Services, July 1999.

11. T. Lillesand and R. Kiefer, *Remote Sensing and Image Interpretation*, (New York: John Wiley & Sons, 1987) 403.

12. Personal Communication, Lynn Calvert, Lockheed Martin Utility Services, July 1999.

13. M. Molbert, "The Eurodif Program," in *Recent Developments in Uranium Enrichment*, ed. J.R. Merriman and M. Benedict, Vol. 78 (NY: American Institute of Chemical Engineers, 1982) 221. This reference quotes a below-ceiling temperature of 80 °C for the Tricastin plant.I conservatively adopt a lower value of 60 °C in all estimates.

14. I used the LANDSAT archives at http://origin.eosat.com.

15. B. Clark, "New Lookup Tables," EOSAT LANDSAT Technical Notes, (August 1996), 1:4. The LANDSAT calibration procedure first converts the raw pixel value, an 8-bit integer, into a radiance value using a standard set of constants. Next the radiance value is converted to a temperature. For the radiance λ, $(mW/(cm^2 \cdot sr \cdot \mu m)$ we have: $\lambda = \lambda_{min} + \frac{\lambda_{max} - \lambda_{min}}{q_{max}} \bullet DN = 0.1238 + 0.00561 DN$,

where $\lambda_{min}, \lambda_{max}$ are respectively the minimum and maximum radiance values from the scene header, DN is the raw 8 bit integer band 6 digital count, (0-255), and q_{max} = 255 is the maximum possible value of DN. The formula for converting the derived radiance value to a Kelvin temperature T is:

$$T = \frac{K_2}{1n\left(\frac{K_1}{\lambda} + 1\right)}$$ where λ is the radiance, and the numerical constants

are $K_1 = 60.776 mW/(cm^2 \cdot sr \cdot \mu m)$ and K_2= 1260.56K for LANDSAT-5 data.

16. A one percent change in the value of the emissivity corresponds to a less than 1°C change in the reconstructed temperature, in the temperature range 0-50°C.

17. B. Clark, op. cit.

18. The roof consists of "a few inches" of composite material, according to Portsmouth site officials.

19. M. Ozisik, *Basic Heat Transfer*, (New York: McGraw Hill, 1977), 8.

20. J. A. Duffie and W. A. Beckman, *Solar Engineering of Thermal Processes*, (New York: John Wiley and Sons, 1980), Table 2.5.1, p. 44, and Table 2.13.1 p. 78.

21. This agreement is fortuitous, since the actual solar absorptivity is unknown -- however this reasonable absorptivity value gives good agreement with the data.

22. It should be noted that this type of change is difficult to accomplish in large gaseous diffusion plants, primarily because of the large inventories of product in the cascade and the long time required to achieve equilibrium in the system.